Cancer Research

ADAPT, a Novel Scaffold Protein-Based Probe for Radionuclide Imaging of Molecular Targets That Are Expressed in Disseminated Cancers

Javad Garousi[1], Sarah Lindbo[2], Johan Nilvebrant[2], Mikael Åstrand[2], Jos Buijs[1], Mattias Sandström[1], Hadis Honarvar[1], Anna Orlova[3], Vladimir Tolmachev[1], and Sophia Hober[2]

Abstract

Small engineered scaffold proteins have attracted attention as probes for radionuclide-based molecular imaging. One class of these imaging probes, termed ABD-Derived Affinity Proteins (ADAPT), has been created using the albumin-binding domain (ABD) of streptococcal protein G as a stable protein scaffold. In this study, we report the development of a clinical lead probe termed ADAPT6 that binds HER2, an oncoprotein overexpressed in many breast cancers that serves as a theranostic biomarker for several approved targeting therapies. Surface-exposed amino acids of ABD were randomized to create a combinatorial library enabling selection of high-affinity binders to various proteins. Furthermore, ABD was engineered to enable rapid purification, to eradicate its binding to albumin, and to enable rapid blood clearance. Incorporation of a unique cysteine allowed site-specific conjugation to a maleimido derivative of a DOTA chelator, enabling radionuclide labeling, ^{111}In for SPECT imaging and ^{68}Ga for PET imaging. Pharmacologic studies in mice demonstrated that the fully engineered molecule ^{111}In/^{68}Ga-DOTA-$(HE)_3$-ADAPT6 was specifically bound and taken up by HER2-expressing tumors, with a high tumor-to-normal tissue ratio in xenograft models of human cancer. Unbound tracer underwent rapid renal clearance followed by high renal reabsorption. HER2-expressing xenografts were visualized by gamma-camera or PET at 1 hour after infusion. PET experiments demonstrated feasibility for discrimination of xenografts with high or low HER2 expression. Our results offer a preclinical proof of concept for the use of ADAPT probes for noninvasive *in vivo* imaging. *Cancer Res; 75(20); 4364–71. ©2015 AACR.*

Introduction

Specific radionuclide imaging of therapeutic molecular targets *in vivo* may provide a noninvasive tool for repeatable determination of their expression levels in disseminated cancer to stratify patients for a targeted therapy (1).

Radiolabeled therapeutic monoclonal antibodies have demonstrated utility in visualization of molecular targets (2–4). However, poor extravasation and penetration of intact antibodies into tumor masses in combination with slow clearance from blood and tissues (5) cause modest imaging contrast. Besides, antibodies as well as other proteins with molecular weights over 45 kDa accumulate in tumors unspecifically (6), which may cause false-positive findings. The use of smaller antibody fragments improves tumor-to-organ radioactivity concentration ratios, and therefore imaging contrast (1). This creates preconditions for better sensitivity. Mathematical modeling suggests that the smaller the imaging agent is, the better the targeting would be if the affinity is high enough (7). The smallest immunoglobulin-based imaging agents utilize camelid VHH fragments (15 kDa) and demonstrate very good imaging properties (8). Still, further size reduction is desirable.

A possible way to generate high-affinity targeting proteins is to combine molecular display techniques (e.g., phage, ribosomal, yeast, or bacterial display) with the use of engineered scaffold proteins (9). Scaffold proteins contain a robust structurally defined framework, which provides rigidity, and a variable surface area, where amino acids are randomized to create libraries for selection of binders. The use of scaffold proteins has enabled the generation of binders with small size (4–20 kDa), well-defined specificity and low nanomolar or subnanomolar affinity. The first scaffold protein for molecular imaging was an affibody molecule targeting HER2, a receptor tyrosine kinase that is overexpressed in cancer and serves as a target for several mAbs and tyrosine kinase inhibitors (10). In preclinical models, this scaffold protein has demonstrated tumor-to-organ ratios exceeding those of monoclonal antibodies by one-two orders of magnitude (11). Clinical studies have confirmed the feasibility of imaging of HER2-expressing metastases using affibody molecules within hours after injection (12). Affibody molecules have also demonstrated successful preclinical imaging of other molecular targets, including

[1]Department of Immunology, Genetics and Pathology, Uppsala University, Uppsala, Sweden. [2]Department of Protein Technology, KTH Royal Institute of Technology, Stockholm, Sweden. [3]Preclinical PET Platform, Department of Medicinal Chemistry, Uppsala University, Uppsala, Sweden.

Note: Supplementary data for this article are available at Cancer Research Online (http://cancerres.aacrjournals.org/).

J. Garousi, S. Lindbo, V. Tolmachev, and S. Hober contributed equally to this article.

Corresponding Author: Vladimir Tolmachev, Uppsala University, Dag Hammarsjold vag 20, Uppsala Sr 752 85, Sweden. Phone: 46-04-525-0782; Fax: 46-471-3432; E-mail: vadimir.tolmachev@igp.uu.se

doi: 10.1158/0008-5472.CAN-14-3497

EGFR (13), HER3 (14), IGF-1R (15), and PDGFRβ (16). Several other targeting scaffold-based proteins, such as anticalins (17), cysteine-knot peptides (18), fibronectin domains (19), and designed ankyrin repeats (20) have successfully been used for imaging of therapeutic targets in preclinical studies. Thus, the use of engineered scaffold proteins is a promising approach for development of imaging agents.

Success of imaging depends both on the binding site and the scaffold part of a protein. The binding site determines affinity and specificity of the targeting. The scaffold provides robustness but may also be involved in off-target interactions, such as binding to blood proteins and normal tissues. Extending the scaffold repertoire increases chances for success in selection of an appropriate imaging agent. In this study, we investigated the potential of the albumin-binding domain (ABD) of streptococcal protein G as a scaffold for development of an imaging agent providing a high contrast. ABD is a small (46 amino acids) protein with a three-helical structure, which is independent of disulfide bonds (21). Important features of ABD include a high melting point, high water solubility, and capacity of high-fidelity refolding after thermal or chemical denaturation (21).

Earlier, we have used a fusion to ABD to modify biodistribution of therapeutic affibody molecules by binding to albumin *in vivo* (22). These studies have demonstrated that ABD-containing conjugates can be labeled at elevated temperatures without losing specificity to albumin. Furthermore, a second specificity (to TNFα and HER3) has been engineered into ABD variants to create potential therapeutics with long residence time in circulation (23, 24). However, an imaging agent should have a short residence time in blood to avoid a high background during imaging. To fulfill this requirement, binding to albumin should be eradicated.

To test the hypothesis that ABD-derived targeting proteins (designated ADAPTs, ABD-Derived Affinity ProTeins) can be used for high-contrast *in vivo* imaging, a new agent was developed. As a molecular target, HER2 was chosen. HER2 is the molecular target for several therapies in breast cancer (25) and detection of HER2 expression in tumors is required to select anti-HER2 therapy (26). Thus, an efficient HER2 imaging agent would be useful for the development of personalized therapy of breast cancer. Because HER2 expression in normal adult tissues is very low (27), the biodistribution of an anti-HER2 ADAPT would depend more on the physical, chemical, and biologic properties of the scaffold than on its on-target interactions with HER2 expressed in healthy tissues. This provides an advantage in initial studies of novel targeting agents. The selection of ADAPT molecules with affinity toward HER2 is described elsewhere (28).

Materials and Methods

All animal experiments were performed in accordance with national legislation on laboratory animal's protection and have been approved by the Ethics Committee for Animal Research in Uppsala. Detailed descriptions of materials, equipments, and methods used in this study are given in the Supplementary Data.

Cell culture

For *in vitro* studies and for *in vivo* models with high HER2 expression, SKOV-3 human ovarian cancer cells (~1.6×10^6 receptors/cell; ref. 29) were used. To model tumors with low target expression, colorectal carcinoma LS174T cells (~3.9×10^4 receptors/cell; ref. 29) were used. HER2-negative Ramos lymphoma cells were used for implantation of HER2-negative control xenografts. All cell lines were from the ATCC. Immediately before experiment, HER2 expression in the cell lines was confirmed by measurement of specific binding of radiolabeled anti-HER2 affibody molecule. Cells were cultured in RPMI medium (Flow Irvine), supplemented with 10% fetal calf serum (Sigma), 2 mmol/L L-glutamine, and PEST (penicillin, 100 IU/mL, and streptomycin, 100 mg/mL; Biokrom Kg).

Tracer design, production, and labeling

The binding of the selected molecule, $ADAPT_{ERBB2\text{-}FACS\text{-}6}$, to albumin was deleted by complementing the substitution L37R (28) at the albumin-binding surface with two alanine substitutions (S18Y20). The novel molecule is denoted ADAPT6. A GCSSHEHEHEDEAVDANS-sequence was introduced at the N-terminus both as a tag for immobilized metal ion affinity chromatography (IMAC) purification and as a biodistribution modifier (30). The variant was designated as C-$(HE)_3$-ADAPT6. In addition, an ADAPT6 molecule with an N-terminal GSSHHHHHHDEAVDANS-sequence was also produced for blocking experiments, H_6-ADAPT. For site-specific labeling, a maleimido-derivative of the versatile DOTA-chelator was conjugated to the unique cysteine introduced at the N-terminus of the $(HE)_3$-ADAPT6. The conjugate was designated as DOTA-C-$(HE)_3$-ADAPT6. The identity of the conjugate was confirmed by liquid chromatography-electrospray ionization mass spectrometry (LC/ESI-MS). Purity of the conjugate was determined by reversed phase high-performance liquid chromatography (RP-HPLC). The thermal stability and secondary structure of DOTA-C-$(HE)_3$-ADAPT6 and H_6-ADAPT6 were determined using a JASCO J-810 spectropolarimeter (JASCO). Binding of DOTA-C-$(HE)_3$-ADAPT6 and H_6-ADAPT6 to HER2 and human serum albumin (HSA) was evaluated on a ProteOn XPR36 Protein interaction array system (Bio-Rad). For experimental details, see Supplementary Data.

For labeling of DOTA-C-(HE)3-ADAPT6 with ^{111}In, the lyophilized protein (50 μg) was reconstituted in 80 μL of 0.2 mol/L ammonium acetate, pH 5.5, mixed with 67 μL of ^{111}In stock solution (30–60 MBq), and incubated at 90°C for 35 minutes.

For labeling with ^{68}Ga, lyophilized DOTA-C-$(HE)_3$-ADAPT6 (50 μg) was reconstituted in 100 μL 1.25 mol/L sodium acetate buffer, pH 3.6. ^{68}Ga, up to 3 MBq per microgram of DOTA-C-$(HE)_3$-ADAPT6, was added to the mixture. The mixture was incubated at 95°C for 30 minutes. After labeling, the conjugate was purified using a NAP-5 size-exclusion column equilibrated with PBS.

Measurements of labeling yield and radiochemical purity of conjugates were performed by radioinstant thin layer chromatography (ITLC) cross-validated by radio–SDS-PAGE, as described earlier (31).

To evaluate the stability of the label, the conjugates were incubated at room temperature in a 500-fold molar excess of EDTA for 1 hour and analyzed using radio-ITLC. The experiments were performed in duplicate. In control experiments, the conjugates were incubated with PBS only.

In vitro cell binding and processing of radiolabeled ADAPT6

Affinity of binding of radiolabeled ^{111}In-DOTA-C-$(HE)_3$-ADAPT6 to HER2-expressing cells was measured using LigandTracer

Yellow instrument (Ridgeview Instruments AB) and analyzed by Interaction Map software (Ridgeview Diagnostics AB) as described by Björkelund and colleagues (32). Specificity of ^{111}In-DOTA-C-(HE)$_3$-ADAPT6 binding to HER2-expressing cells and cellular processing of the bound conjugate was evaluated according to methods described earlier (33). Briefly, the saturability of ^{111}In-DOTA-C-(HE)$_3$-ADAPT6 to HER2-expressing cells was tested by saturating receptors by addition of a 100-fold molar excess of nonlabeled H$_6$-ADAPT6, an anti-HER2 Z$_{HER2:342}$ affibody molecule or the anti-HER2 antibody trastuzumab. Internalization of ^{111}In-DOTA-C-(HE)$_3$-ADAPT6 by HER2-expressing cancer cells was measured by the acid wash method (33). For experimental details, see Supplementary Data.

In vivo evaluation of radiolabeled DOTA-C-(HE)$_3$-ADAPT6

Euthanasia was performed under Rompun/Ketalar anesthesia. Animals were purchased from Taconic M&B.

A group of four mice was used for each data point. The mice were euthanized at predetermined time points post-injection (p.i.) by overdosing of anesthesia followed by heart puncture and exsanguination. Blood and organ samples were collected and their weight and radioactivity were measured. Organ uptake values were calculated as the percentage of injected activity per gram of tissue (%IA/g).

A study in normal NMRI mice was performed to evaluate the biodistribution pattern of ^{111}In-DOTA-C-(HE)$_3$-ADAPT6, particularly the blood clearance rate. Female NMRI mice (average weight 24 $\pm$ 2 g) were injected with 30 kBq (1 μg) of ^{111}In-DOTA-C-(HE)$_3$-ADAPT6 in 100 μL PBS and biodistribution was measured at 1, 4, and 24 hours p.i.

Targeting properties and *in vivo* specificity of ^{111}In-DOTA-C-(HE)$_3$-ADAPT6 were evaluated in female BALB/C nu/nu mice bearing SKOV-3 xenografts. For establishing HER2-positive xenografts, 10^7 SKOV-3 cells were s.c. implanted in the right hind leg. For HER2-negative controls, 5×10^6 Ramos cells were s.c. implanted. At the time of experiments, the average animal weight was 19 $\pm$ 1 g. The average weight of xenografts was 0.31 $\pm$ 0.18 g and 0.11 $\pm$ 0.09 g for SKOV-3 and Ramos, respectively. ^{111}In-DOTA-C-(HE)$_3$-ADAPT6 (30 kBq, 3 μg in 100 μL PBS) was injected i.v. (tail vein) in three groups of mice with SKOV-3 xenografts and one control group with Ramos xenografts. To saturate HER2 receptors in tumors, another control group of mice was injected with ^{111}In-DOTA-C-(HE)$_3$-ADAPT6 (30 kBq) at the protein dose of 300 μg. Biodistribution was measured at 1, 4, and 24 hours p.i. Biodistribution in control groups was measured at 1 hour p.i.

Targeting of human tumor xenografts with high (SKOV-3) and low (LS174T) expression of HER2 in mice using ^{68}Ga-DOTA-C-(HE)$_3$-ADAPT6 was compared at 1 hour p.i. The goal of this experiment was to confirm that DOTA-C-(HE)$_3$-ADAPT6 labeled with positron-emitting nuclide^{68}Ga can specifically target HER2-expressing xenografts, and that the discrimination between tumors with high and low HER2 expression is better at a higher injected protein dose. At the time of experiments, the average animal weight was 19 $\pm$ 1 g in both groups. The average weight of SKOV-3 xenografts was 0.21 $\pm$ 0.09 g and 0.3 $\pm$ 0.2 g for LS174T xenografts. All animals were injected with 300 kBq ^{68}Ga-DOTA-C-(HE)$_3$-ADAPT6 in 100 μL PBS. For each type of xenograft, the injected protein dose was adjusted with unlabeled DOTA-C-(HE)$_3$-ADAPT6 to 1 μg for one group and to 15 μg for the other group.

Imaging

Imaging was performed to obtain a visual confirmation of *ex vivo* measurements. For gamma-camera imaging, two mice bearing SKOV-3 xenografts were injected with 5.7 MBq ^{111}In-DOTA-C-(HE)$_3$-ADAPT6 at protein dose 3 μg/mouse and one with 5.7 MBq at protein dose 300 μg. Immediately before imaging (1 hour p.i.), the animals were sacrificed by overdosing Ketalar–Rompun. The imaging experiment was performed using a GE Infinia gamma-camera equipped with a medium energy general purpose (MEGP) collimator. Static images (30 minutes) were obtained with a zoom factor of three in a 256 $\times$ 256 matrix.

For PET imaging, one mouse with SKOV-3 xenograft and one with LS174T xenograft were injected with 15 MBq ^{68}Ga-DOTA-C-(HE)$_3$-ADAPT6 (15 μg). Animals were sacrificed and imaged at 1 hour p.i. The PET imaging was performed using a clinical scanner, GE Discovery VCT PET/CT, in 3D mode with a 30-minute image reconstructed in a 256 $\times$ 256 matrix with a 30-cm field of view.

Results

Tracer design, production, and labeling

Analytic RP-HPLC showed a purity of more than 95% for DOTA-C-(HE)$_3$-ADAPT6 (Supplementary Fig. S1). The molecular mass of DOTA-C-(HE)$_3$-ADAPT6 was determined by mass spectrometry analysis and showed an excellent agreement with the theoretical value (Supplementary Fig. S2, expected 7559 Da, found 7560 Da). Circular dichroism measurements (Supplementary Fig. S3) revealed a high α-helical content and high-fidelity refolding after heating to 90°C, both in agreement with the parental protein scaffold. The melting temperature was 68°C (Supplementary Fig. S4). The binding affinity (K_D) to human recombinant HER2 was 2.5 nmol/L according to SPR analysis (Fig. 1A; Supplementary Table S1). Deletion of albumin binding was verified by SPR analysis where no reactivity against HSA was detected (Fig. 1B).

The labeling yield was 98.9% $\pm$ 0.7% for ^{111}In and 98.3% $\pm$ 1.7% for ^{68}Ga. The identity of conjugates was confirmed by radio–SDS-PAGE (Supplementary Fig. S5). A challenge with 500-fold excess of EDTA during 2 hours did not reveal any release of radioactivity from the conjugates. Specific activities of 1 MBq/μg (7.6 GBq/μmol) and 2.1 MBq/μg (16 GBq/μmol) were obtained for ^{111}In and ^{68}Ga-labeled conjugates, respectively.

In vitro cell binding and processing of radiolabeled ADAPT6

According to Interaction Map analysis (Supplementary Figs. S6 and S7), binding of the ^{111}In-DOTA-C-(HE)$_3$-ADAPT6 to living HER2-expressing SKOV-3 cells had an affinity (K_D) of 1.13 $\pm$ 0.05 nmol/L.

In vitro saturation experiments (Fig. 1C) demonstrated that addition of a 100-fold molar excess of the nonlabeled ADAPT6 significantly ($P < 0.05$) reduced the binding of ^{111}In-DOTA-C-(HE)$_3$-ADAPT6 to HER2-expressing SKOV-3 cells. This demonstrated a saturable character of the binding, proving its specificity. Moreover, the binding of ^{111}In-DOTA-C-(HE)$_3$-ADAPT6 was prevented by addition of an excess of trastuzumab. However, adding an excess amount of an anti-HER2 Z$_{HER2:342}$ affibody molecule did not affect the binding of ^{111}In-DOTA-C-(HE)$_3$-ADAPT6. This shows that ADAPT6 competes for the binding site with trastuzumab but not with the Z$_{HER2:342}$ affibody molecule, which is in agreement with previous results (28). Binding of ^{111}In-DOTA-C-(HE)$_3$-ADAPT6 to LS174T had the same saturability

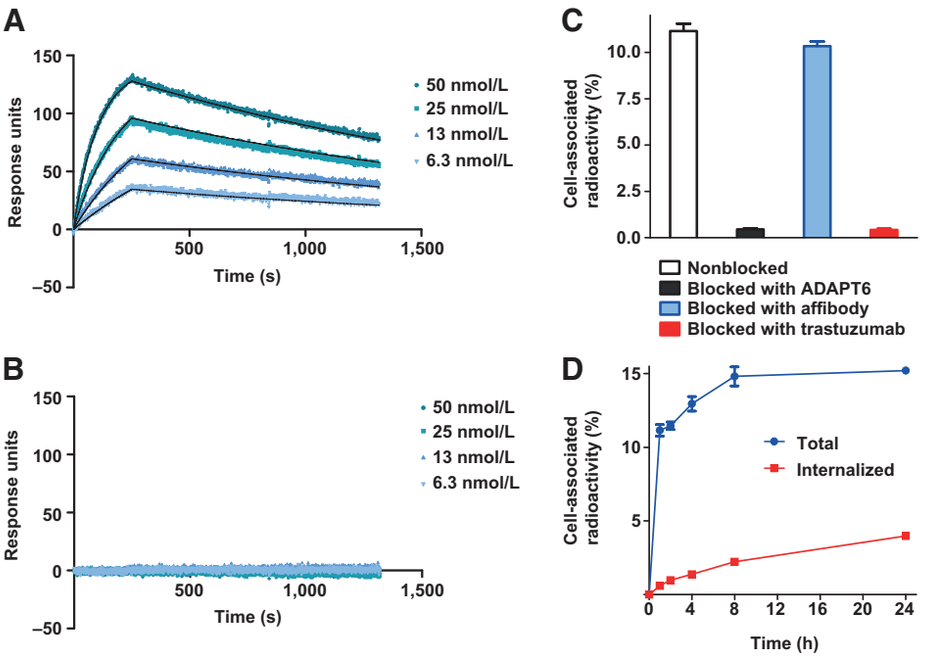

Figure 1.
In vitro characterization of DOTA-C-$(HE)_3$-ADAPT6. SPR sensorgrams of DOTA-C-$(HE)_3$-ADAPT injected over immobilized HER2 (A) and HSA (B). C, specificity of the binding of ^{111}In-DOTA-C-$(HE)_3$-ADAPT6 to HER2-expressing SKOV-3 cells *in vitro*. For the presaturation of HER2, a 100-fold molar excess of nonlabeled H_6-ADAPT6, anti-HER2 $Z_{HER2:342}$ affibody, or trastuzumab was added. Data, mean ± SD ($n = 3$). D, cell-associated radioactivity as a function of time during continuous incubation of HER2-expressing SKOV-3 cells with the ^{111}In labeled ADAPT6 molecule. Data, mean ± SD ($n = 3$).

pattern, but the binding to nonsaturated cells was much lower than in case of SKOV3 cells (0.39% ± 0.03% vs. 11.0% ± 0.4% of added radioactivity), reflecting the low HER2 expression in this cell line.

The binding and internalization of ^{111}In-DOTA-C-$(HE)_3$-ADAPT6 by SKOV-3 cells is shown in Fig. 1D. The internalization of the ADAPT6 protein was slow: Only 5% and 26% of the total bound radioactive molecules were internalized after one and 24 hours of incubation, respectively.

In vivo evaluation of radiolabeled DOTA-C-$(HE)_3$-ADAPT6

A first evaluation of ^{111}In-DOTA-C-$(HE)_3$-ADAPT6 was performed in normal NMRI mice (Fig. 2). The rapid clearance of the tracer from blood (0.36 ± 0.09 %IA/g at 1 hour p.i.) confirmed that there was no residual binding to albumin. ^{111}In-DOTA-C-$(HE)_3$-ADAPT6 also cleared rapidly from other organs and tissues (uptake of less than 1 %IA/g at 1 hour p.i.) except from kidneys.

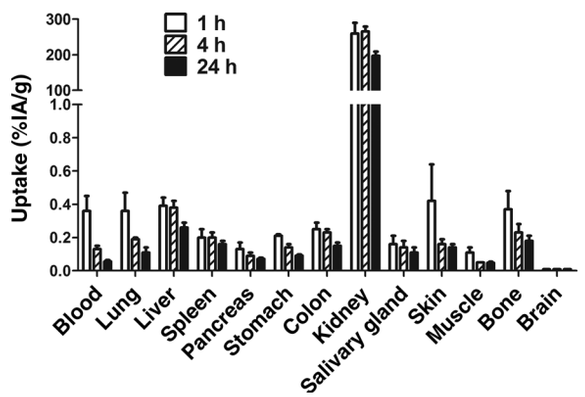

Figure 2.
Biodistribution of ^{111}In-DOTA-C-$(HE)_3$-ADAPT6 in female normal (NMRI) mice. Data, mean %IA/g ± SD ($n = 4$).

Low radioactivity in the gastrointestinal tract including content (0.44% ± 0.08% of injected activity at 1 hour p.i.) suggested that hepatobiliary excretion played a minor role in the clearance. The renal uptake was high, 259 ± 30 %IA/g at 1 hour p.i.

Biodistribution of ^{111}In-DOTA-C-$(HE)_3$-ADAPT6 in BALB/C nu/nu mice bearing SKOV-3 xenografts is shown in Figs. 3 and 4. The specificity of HER2 targeting *in vivo* was demonstrated by saturation of HER2 receptors and by the use of HER2-negative Ramos xenografts (Fig. 3). The use of a saturating amount (300 μg) of nonlabeled H_6-ADAPT6 resulted in a reduction of tumor uptake of ^{111}In-DOTA-C-$(HE)_3$-ADAPT6 from 19 ± 6 to 3.3 ± 0.4 %IA/g ($P < 0.005$). Some reduction of the uptake was observed also in kidneys ($P < 0.05$). Interestingly, the uptake in spleen was significantly ($P < 0.05$) higher in mice injected with 300 μg

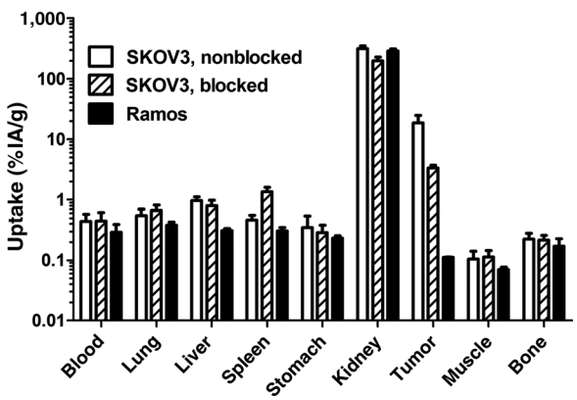

Figure 3.
In vivo targeting specificity of ^{111}In-DOTA-C-$(HE)_3$-ADAPT6 (3 μg) in mice bearing SKOV-3 xenografts at 1 hour p.i. The blocked group was coinjected with an excess amount (300 μg) of nonlabeled H_6-ADAPT6 molecule. Ramos xenografts were used as a HER2-negative control. Data, mean %IA/g ± SD ($n = 4$). Please note the logarithmic scale.

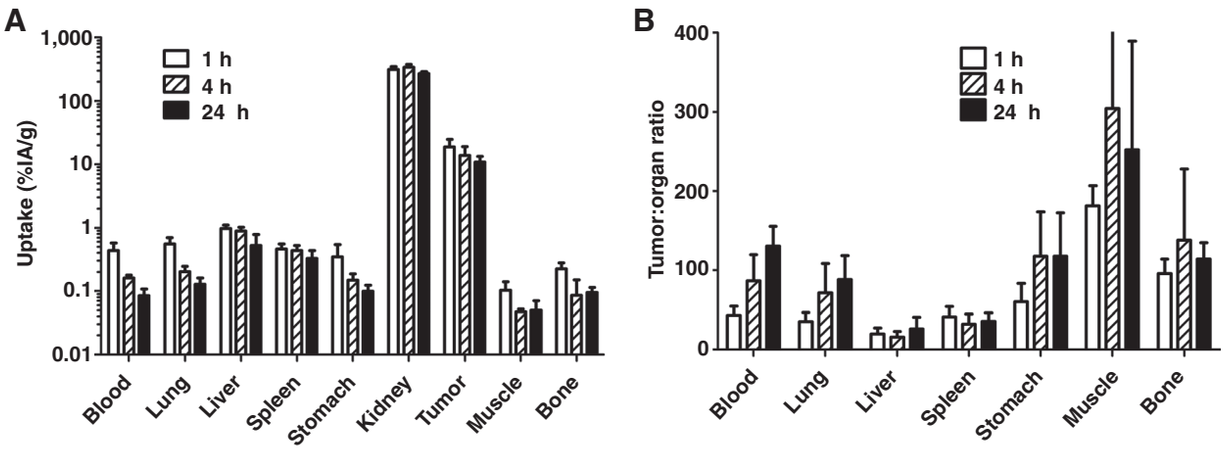

Figure 4.
Biodistribution (A) and tumor-to-organ ratios (B) of ^{111}In-DOTA-C-(HE)$_3$-ADAPT6 in mice bearing SKOV-3 xenografts. Data, mean ± SD ($n = 4$). Please note the logarithmic scale in A.

H_6-ADAPT6. Uptake in Ramos xenografts (0.112 ± 0.002 %IA/g) was significantly ($P < 0.05$) lower than uptake in SKOV-3 xenografts, on the same level as in muscles.

The biodistribution in normal organs (Fig. 4A) was characterized by rapid clearance from normal tissues except from kidneys and was in an excellent agreement with the data for NMRI mice. The tumor uptake was 18.7 ± 6.1, 13.9 ± 5.2, and 10.8 ± 2.5 %IA/g at 1, 4, and 24 hours p.i., respectively. Although the time points do not differ significantly ($P > 0.05$), there is a clear trend that tumor uptake decreases over time. Such biodistribution pattern provided high tumor-to-organ ratios already at 1 hour p.i. (Fig. 4B). For example, the tumor-to-blood ratio was as high as 43 ± 11 at this time point. At later time points, there was a significant ($P < 0.05$) increase only in tumor-to-blood and tumor-to-lung ratios.

Biodistribution and tumor-to-organ ratios of ^{68}Ga-DOTA-C-(HE)$_3$-ADAPT6 in BALB/C nu/nu mice bearing SKOV-3 (high HER2 expression) and LS174T (low HER2 expression) xenografts at 1 hour p.i. are shown in Tables 1 and 2. At both injected doses (1 or 15 μg), the uptake in SKOV-3 xenografts was much higher than in LS174T xenografts, which shows that tumor accumulation was dependent on target expression level. In both xenograft models, an increase of injected protein dose caused significant decrease of uptake, suggesting saturable uptake. At higher injected protein dose, the difference between xenografts with high and low HER2 expression was bigger (9.3-fold) than at lower dose (3.6-fold). Although uptake in SKOV-3 xenografts was lower at 15 μg, the tumor-to-organ ratios were not lower (Table 2).

Imaging

Experimental imaging (Fig. 5) confirmed the biodistribution results. The only normal organ with high uptake of radioactivity was kidney. No other organs were visualized. SKOV-3 xenografts with high HER2 expression were clearly visualized with a high contrast using 3 μg ^{111}In-DOTA-C-(HE)$_3$-ADAPT6. Saturation of receptors with DOTA-C-(HE)$_3$-ADAPT6 caused dramatic decrease of tumor uptake (Fig. 5A). PET imaging (Fig. 5B) demonstrated that xenografts with high (SKOV-3) and low (LS174T) HER2 expression could be easily distinguished using 15 μg ^{68}Ga-DOTA-C-(HE)$_3$-ADAPT6.

Discussion

Both theoretical calculations and experimental data (5, 7, 34) suggest that size reduction is the most promising way to increase imaging contrast provided by proteinaceous imaging agents.

Table 1. Biodistribution of ^{68}Ga-DOTA-C-(HE)$_3$-ADAPT6 in BALB/C nu/nu mice bearing SKOV-3 xenografts (high HER2 expression) and LS174T (low HER2 expression) at 1 hour p.i.

	SKOV3 xenografts		LS174T xenografts	
	1 μg	15 μg	1 μg	15 μg
Blood	0.59 ± 0.07	0.50 ± 0.06	0.60 ± 0.09	0.6 ± 0.2
Lung	0.70 ± 0.02	0.53 ± 0.06	0.67 ± 0.09	0.7 ± 0.2
Liver	1.7 ± 0.1	1.21 ± 0.05	1.8 ± 0.1	1.6 ± 0.1
Spleen	0.62 ± 0.05	0.50 ± 0.07	0.74 ± 0.07	0.56 ± 0.34
Stomach	0.63 ± 0.11	0.35 ± 0.07	0.54 ± 0.06	0.36 ± 0.09
Kidney	308 ± 24	277 ± 5	323 ± 27	311 ± 31
Tumor	10.3 ± 1.0[a,c]	8.4 ± 0.6[d]	2.9 ± 0.5[b]	0.9 ± 0.6
Muscle	0.18 ± 0.01	0.12 ± 0.02	0.14 ± 0.02	0.14 ± 0.03
Bone	0.5 ± 0.1	0.34 ± 0.07	0.5 ± 0.1	0.4 ± 0.1

NOTE: Data are presented as an average %IA/g and SD for four mice.
Difference was significant ($P < 0.05$) between:
[a]Injected dose of 1 and 15 μg in SKOV3 xenografts.
[b]Injected dose of 1 and 15 μg in LS174T xenografts.
[c]SKOV3 and LS174T xenografts at injected dose of 1 μg.
[d]SKOV3 and LS174T xenografts at injected dose of 15 μg.

Table 2. Tumor-to-organ ratios of ^{68}Ga-DOTA-C-(HE)$_3$-ADAPT6 in BALB/C nu/nu mice bearing SKOV-3 xenografts (high HER2 expression) and LS174T (low HER2 expression) at 1 hour p.i.

	SKOV3 xenografts		LS174T xenografts	
	1 μg	15 μg	1 μg	15 μg
Blood	17.5 ± 0.3	17 ± 2	4.8 ± 0.2	1.5 ± 0.8
Lung	15 ± 1	16 ± 1	4.3 ± 0.2	1.4 ± 0.7
Liver	6.0 ± 0.1	7.0 ± 0.4	1.6 ± 0.2	0.6 ± 0.4
Spleen	17 ± 2	17 ± 1	3.9 ± 0.4	2.1 ± 1.0
Stomach	16 ± 1	24 ± 4	5 ± 1	2 ± 1
Kidney	0.034 ± 0.005	0.030 ± 0.003	0.009 ± 0.002	0.003 ± 0.002
Muscle	56 ± 9	70 ± 6	21 ± 4	7 ± 4
Bone	20 ± 4	25 ± 4	7 ± 3	2 ± 1

NOTE: Data are presented as an average value and SD for four mice.

ADAPT (scaffold size 5.1 kDa without linkers and tags) has a size advantage in comparison with many other scaffold proteins, such as affibody molecules (7 kDa), designed ankyrin repeat proteins (14 kDa), anticalins (20 kDa), fibronectin domains (adnectins) (10 kDa), and VHHs (15 kDa). Knottins (4 kDa) are smaller, but they and many of the other scaffold proteins contain cysteines. The cysteine-free structure of ADAPT enables the use of oxidizing and reducing conditions during conjugation and labeling without affecting the structure of the domain. Moreover, the possibility to introduce a unique cysteine, as in this study, provides easy site-specific conjugation of chelators and other prosthetic groups that gives homogenous ADAPT conjugates. However, these potential advantages of ABD-based imaging agents could be realized only with three preconditions:

1. Generation of ABD derivatives with affinity in the range of 10 pmol/L to 10 nmol/L (35) to therapeutic targets should be possible;
2. Binding to albumin should be reduced to a level that permits rapid clearance from blood;
3. Off-target interaction of the scaffold should not cause any noticeable uptake in normal tissues.

An optimal affinity (K_D) for imaging agents should be in the range between 10 pmol/L and 10 nmol/L. If K_D is lower than 10 pmol/L (very high affinity), pharmacokinetics of the agent would depend heavily on blood flow or vascular permeability. Furthermore, if K_D is greater than 10 nmol/L, the off-rate will be too fast, and the retention at specific binding sites might be insufficient (35). This and previous studies (21, 23, 24) have demonstrated that selection of ADAPT binders with an optimal affinity to several therapeutic targets (HER2, HER3, and TNFα) is possible. This study has demonstrated that reduction of the affinity to albumin to a nonmeasurable level is also possible. The data from the first animal study (Fig. 2) demonstrated rapid clearance from blood. Furthermore, these data showed very low uptake in normal tissues (except kidneys), which suggests absence of noticeable off-target interactions. The high renal uptake is a general feature of all radiometal-labeled scaffold proteins, including nanobodies (36), affibody molecules (13–15), fibronectin domains (19), and designed ankyrin repeats (20). This uptake is caused by reabsorption from primary urine in proximal tubuli. After rapid internalization and proteolytic degradation, bulky hydrophilic radiometabolites get trapped inside proximal tubili cells. However, renal metastases are rather rare, and the well-defined shape of kidneys excludes false-positive findings. Moreover, our clinical study with affibody molecules suggests that high renal uptake does not prevent visualization of adrenal metastases and absorbed doses to kidneys permit multiple imaging procedures (12). Considerations concerning dosimetry aspects of high renal uptake are presented in Supporting Information. In addition, earlier we have shown for affibody molecules that the use of radiohalogen labels yields lipophilic radiometabolites, which "leak" rapidly from kidneys (11, 37). In the case of slow internalization by cancer cells, the use of radiohalogen labels has very little influence on tumor uptake of affibody molecules (11, 37). As internalization of ADAPT6 is also slow (Fig. 1D), the use of nonresidualizing radiohalogen labels may provide ADAPT-based

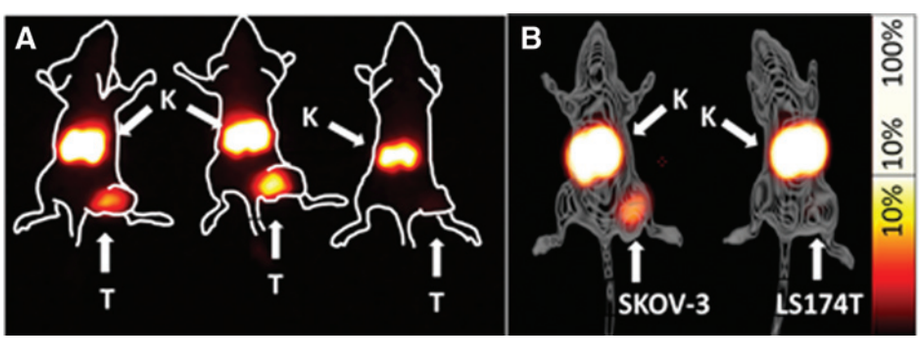

Figure 5.
Imaging of HER2 expression in xenografts using radiolabeled DOTA-C-(HE)$_3$-ADAPT6. A, gamma-camera imaging of SKOV-3 xenografts using ^{111}In-DOTA-C-(HE)$_3$-ADAPT6 (3 μg). Contours were derived from a digital photograph and superimposed over images to facilitate interpretation. A control animal (right) was injected with a saturating amount of nonlabeled ADAPT6. B, PET/CT imaging of SKOV-3 (high expression) and LS174T (low expression) xenografts using ^{68}Ga-DOTA-C-(HE)$_3$-ADAPT6. Injected protein dose was 15 μg. Arrows are pointing at tumors (T) and kidneys (K).

imaging agents with high uptake in tumors but low radioactivity retention in kidneys.

Both *in vivo* specificity tests (saturation and the use of HER2-negative xenografts) confirmed highly specific targeting of HER2-positive xenografts using ^{111}In-DOTA-C-$(HE)_3$-ADAPT6 (Fig. 3). Interestingly, the spleen uptake was increased in a saturation experiment. This might be due to weak cross-reactivity with other molecular targets expressed in the spleen or with a target that is taken up by the spleen. Such weak cross-reactivity is primarily manifested when a large amount of conjugate is injected (For more detailed consideration see Supplementary Information. Considerations concerning splenic uptake at high injected dose of ^{111}In-DOTA-C-$(HE)_3$-ADAPT6). Importantly, the uptake in HER2-positive xenografts exceeded uptake in negative ones by more than 160-fold. This demonstrated absence of an enhanced permeability and retention effect for ADAPTs, and excludes false-positive findings due to unspecific uptake in tumors. The uptake of the ADAPT in SKOV-3 xenografts (19 ± 6 %IA/g at 1 hour) was at the same level as for radiometal-labeled HER2-targeting affibody molecules (17 ± 2 %IA/g; ref. 38), and exceeded reported uptake for DARPins (8.3 ± 2.7 %IA/g; ref. 20) and nanobodies (4.7 ± 0.7 %IA/g; ref. 36) at the same time point in the same xenografts. The data concerning higher tumor uptake of smaller ADAPTs and affibody molecules in comparison with larger DARPins and nanobodies are consistent with a previous comparison with dimeric affibody molecules. It has been shown that the smaller monomers have higher tumor uptake than larger dimers (37). Together, these data suggest that the use of smaller scaffold proteins improves tumor targeting, presumably due to better extravasation. Importantly, clearance of ^{111}In-DOTA-C-$(HE)_3$-ADAPT6 was more rapid than clearance of, for example, affibody molecules. As a result, the highest tumor-to-organ ratios were reached very early (Fig. 4B), which enabled high-contrast imaging already at 1 hour p.i. (Fig. 5A). Ability to provide high-contrast images shortly after injection offers clear clinical and logistical advantages. Importantly, it permits the use of short-lived positron emitting radionuclides for labeling and therefore PET for imaging is feasible (Fig. 5B).

A rapid blood clearance in combination with high affinity might cause equal uptake of an imaging agent in tumors with high and low target expression. However, this limitation can be circumvented by increasing injected protein dose. We have shown this earlier for affibody molecules in preclinical models (39). In this study, an increase of the injected dose from 1 to 15 μg increased the difference in uptake in xenografts with low and high expression from 3-fold to more than 9-fold. This indicates that during possible clinical translation a dose-finding study should be performed to determine an optimal injected dose permitting clear discrimination between tumors with high and low target expression.

In conclusion, ADAPTs can be used as imaging agents that provide high-contrast PET imaging of HER2 expression in cancer shortly after injection. This shows that ADAPT is a very promising novel scaffold for development of imaging agents for personalized cancer treatment.

Disclosure of Potential Conflicts of Interest

J. Buijs is a CTO for Ridgeview Instruments AB. A. Orlova has ownership interest (including patents) and is a consultant/advisory board member for Affibody AB, Sweden. V. Tolmachev has ownership interest (including patents) and is a consultant/advisory board member for Affibody AB, Solna, Sweden. No potential conflicts of interest were disclosed by the other authors.

Authors' Contributions

Conception and design: S. Lindbo, J. Nilvebrant, M. Åstrand, A. Orlova, V. Tolmachev, S. Hober

Development of methodology: J. Garousi, S. Lindbo, J. Nilvebrant, M. Åstrand, H. Honarvar, A. Orlova, V. Tolmachev, S. Hober

Acquisition of data (provided animals, acquired and managed patients, provided facilities, etc.): J. Garousi, J. Nilvebrant, M. Sandström, H. Honarvar, A. Orlova, V. Tolmachev

Analysis and interpretation of data (e.g., statistical analysis, biostatistics, computational analysis): J. Garousi, S. Lindbo, J. Nilvebrant, M. Åstrand, J. Buijs, M. Sandström, H. Honarvar, A. Orlova, V. Tolmachev, S. Hober

Writing, review, and/or revision of the manuscript: J. Garousi, S. Lindbo, J. Nilvebrant, M. Åstrand, J. Buijs, M. Sandström, H. Honarvar, A. Orlova, V. Tolmachev, S. Hober

Administrative, technical, or material support (i.e., reporting or organizing data, constructing databases): V. Tolmachev

Study supervision: M. Sandström, V. Tolmachev, S. Hober

Grant Support

This research was financially supported by grants from the Swedish Cancer Society (grant 2012/354) and the Swedish Research Council (grants 521-2012-2228 and 621-2012-5088).

The costs of publication of this article were defrayed in part by the payment of page charges. This article must therefore be hereby marked *advertisement* in accordance with 18 U.S.C. Section 1734 solely to indicate this fact.

Received December 3, 2014; revised July 18, 2015; accepted July 23, 2015; published OnlineFirst August 21, 2015.

References

1. Tolmachev V, Stone-Elander S, Orlova A. Radiolabelled receptor-tyrosine-kinase targeting drugs for patient stratification and monitoring of therapy response: prospects and pitfalls. Lancet Oncol 2010;11:992–1000.
2. Behr TM, Béhé M, Wörmann B. Trastuzumab and breast cancer. N Engl J Med 2001;345:995–6.
3. Dijkers EC, Oude Munnink TH, Kosterink JG, Brouwers AH, Jager PL, de Jong JR, et al. Biodistribution of ^{89}Zr-trastuzumab and PET imaging of HER2-positive lesions in patients with metastatic breast cancer. Clin Pharmacol Ther 2010;87:586–92.
4. Gaykema SB, Brouwers AH, Lub-de Hooge MN, Pleijhuis RG, Timmer-Bosscha H, Pot L, et al. ^{89}Zr-bevacizumab PET imaging in primary breast cancer. J Nucl Med 2013;54:1014–8.
5. Jain RK. Physiological barriers to delivery of monoclonal antibodies and other macromolecules in tumors. Cancer Res 1990;50(3 Suppl):814s–819s.
6. Wester HJ, Kessler H. Molecular targeting with peptides or peptide-polymer conjugates: just a question of size? J Nucl Med 2005;46:1940–5.
7. Wittrup KD, Thurber GM, Schmidt MM, Rhoden JJ. Practical theoretic guidance for the design of tumor-targeting agents. Methods Enzymol 2012;503:255–68.
8. Chakravarty R, Goel S, Cai W. the "magic bullet" for molecular imaging? Theranostics 2014;4:386–98.
9. Binz HK, Amstutz P, Pluckthun A. Engineering novel binding proteins from nonimmunoglobulin domains. Nat Biotechnol 2005;23:1257–68.
10. Orlova A, Magnusson M, Eriksson TL, Nilsson M, Larsson B, Höidén-Guthenberg I, et al. Tumor imaging using a picomolar affinity HER2 binding affibody molecule. Cancer Res 2006;66:4339–48.
11. Orlova A, Wållberg H, Stone-Elander S, Tolmachev V. On the selection of a tracer for PET imaging of HER2-expressing tumors: direct comparison of a ^{124}I-labeled affibody molecule and trastuzumab in a murine xenograft model. J Nucl Med 2009;50:417–25.

12. Sörensen J, Sandberg D, Sandström M, Wennborg A, Feldwisch J, Tolmachev V, et al. First-in-human molecular imaging of HER2 expression in breast cancer metastases using the ^{111}In-ABY-025 affibody molecule. J Nucl Med 2014;55:730–5.
13. Tolmachev V, Rosik D, Wållberg H, Sjöberg A, Sandström M, Hansson M, et al. Imaging of EGFR expression in murine xenografts using site-specifically labelled anti-EGFR 111In-DOTA-Z EGFR:2377 Affibody molecule: aspect of the injected tracer amount. Eur J Nucl Med Mol Imaging 2010;37:613–22.
14. Orlova A, Malm M, Rosestedt M, Varasteh Z, Andersson K, Selvaraju RK, et al. Imaging of HER3-expressing xenografts in mice using a ^{99m}Tc(CO)$_3$-HEHEHE-Z HER3:08699 affibody molecule. Eur J Nucl Med Mol Imaging 2014;41:1450–9.
15. Orlova A, Hofström C, Strand J, Varasteh Z, Sandstrom M, Andersson K, et al. [99mTc(CO)$_3$]$^+$-(HE)$_3$-ZIGF1R:4551, a new Affibody conjugate for visualization of insulin-like growth factor-1 receptor expression in malignant tumours. Eur J Nucl Med Mol Imaging 2013;40:439–49.
16. Tolmachev V, Varasteh Z, Honarvar H, Hosseinimehr SJ, Eriksson O, Jonasson P, et al. Imaging of platelet-derived growth factor receptor β expression in glioblastoma xenografts using affibody molecule ^{111}In-DOTA-Z09591. J Nucl Med 2014;55:294–300.
17. Terwisscha van Scheltinga AG, Lub-de Hooge MN, Hinner MJ, Verheijen RB, Allersdorfer A, Hülsmeyer M, et al. *In vivo* visualization of MET tumor expression and anticalin biodistribution with the MET-specific anticalin ^{89}Zr-PRS-110 PET tracer. J Nucl Med 2014;55:665–71.
18. Ackerman SE, Currier NV, Bergen JM, Cochran JR. Cystine-knot peptides: emerging tools for cancer imaging and therapy. Expert Rev Proteomics 2014;11:561–72.
19. Hackel BJ, Kimura RH, Gambhir SS. Use of ^{64}Cu-labeled fibronectin domain with EGFR-overexpressing tumor xenograft: molecular imaging. Radiology 2012;263:179–88.
20. Zahnd C, Kawe M, Stumpp MT, de Pasquale C, Tamaskovic R, Nagy-Davidescu G, et al. Efficient tumor targeting with high-affinity designed ankyrin repeat proteins: effects of affinity and molecular size. Cancer Res 2010;70:1595–1605.
21. Nilvebrant J, Hober S. The albumin-binding domain as a scaffold for protein engineering. Comput Struct Biotechnol J 2013;6:e201303009.
22. Tolmachev V, Orlova A, Pehrson R, Galli J, Baastrup B, Andersson K, et al. Radionuclide therapy of HER2-positive microxenografts using a ^{177}Lu-labeled HER2-specific Affibody molecule. Cancer Res 2007;67:2773–82.
23. Nilvebrant J, Alm T, Hober S, Löfblom J. Engineering bispecificity into a single albumin-binding domain. PLoS ONE 2011;6:e25791.
24. Nilvebrant J, Astrand M, Löfblom J, Hober S. Development and characterization of small bispecific albumin-binding domains with high affinity for ErbB3. Cell Mol Life Sci 2013;70:3973–85.
25. Giordano SH, Temin S, Kirshner JJ, Chandarlapaty S, Crews JR, Davidson NE, et al. Systemic therapy for patients with advanced human epidermal growth factor receptor 2-positive breast cancer: American Society Of Clinical Oncology Clinical Practice Guideline. J Clin Oncol 2014;32:2078–99.
26. Wolff AC, Hammond ME, Hicks DG, Dowsett M, McShane LM, Allison KH, et al. Recommendations for human epidermal growth factor receptor 2 testing in breast cancer: American Society of Clinical Oncology/College of American Pathologists clinical practice guideline update. J Clin Oncol 2013;31:3997–4013
27. Natali PG, Nicotra MR, Bigotti A, Venturo I, Slamon DJ, Fendly BM, et al. Expression of the p185 encoded by HER2 oncogene in normal and transformed human tissues. Int J Cancer 1990;45:457–61.
28. Nilvebrant J, Åstrand M, Georgieva-Kotseva M, Björnmalm M, Löfblom J, Hober S. Engineering of bispecific affinity proteins with high affinity for ERBB2 and adaptable binding to albumin. PLoS ONE 2014;9:e103094.
29. Tolmachev V, Tran TA, Rosik D, Sjöberg A, Abrahmsén L, Orlova A. Tumor targeting using Affibody molecules: interplay of affinity, target expression level and binding site composition. J Nucl Med 2012;53:953–60.
30. Hofstrom C, Orlova A, Altai M, Wangsell F, Graslund T, Tolmachev V. Use of a HEHEHE purification tag instead of a hexahistidine tag improves biodistribution of affibody molecules site-specifically labeled with ^{99m}Tc, ^{111}In, and ^{125}I. J Med Chem 2011;54:3817–26.
31. Tolmachev V, Velikyan I, Sandström M, Orlova A. A HER2-binding Affibody molecule labelled with 68Ga for PET imaging: direct *in vivo* comparison with the 111In-labelled analogue. Eur J Nucl Med Mol Imaging 2010;37:1356–67.
32. Björkelund H, Gedda L, Barta P, Malmqvist M, Andersson K. Gefitinib induces epidermal growth factor receptor dimers which alters the interaction characteristics with 125I-EGF. PLoS ONE 2001;6:e24739.
33. Wållberg H, Orlova A. Slow internalization of anti-HER2 synthetic affibody monomer 111In-DOTA-ZHER2:342-pep2: implications for development of labeled tracers. Cancer Biother Radiopharm 2008;23:435–42.
34. Wållberg H, Ståhl S. Design and evaluation of radiolabeled tracers for tumor imaging. Biotechnol Appl Biochem 2013;60:365–83.
35. Eckelman WC, Kilbourn MR, Mathis CA. Discussion of targeting proteins *in vivo*: *in vitro* guidelines. Nucl Med Biol 2006;33:449–51.
36. Vaneycken I, Devoogdt N, Van Gassen N, Vincke C, Xavier C, Wernery U, et al. (2011) Preclinical screening of anti-HER2 nanobodies for molecular imaging of breast cancer. FASEB J 2011;25:2433–46.
37. Tolmachev V, Mume E, Sjöberg S, Frejd FY, Orlova A. Influence of valency and labelling chemistry on *in vivo* targeting using radioiodinated HER2-binding Affibody molecules. Eur J Nucl Med Mol Imaging 2009;36:692–701.
38. Ahlgren S, Orlova A, Wållberg H, Hansson M, Sandström M, Lewsley R, et al. Targeting of HER2-expressing tumors using 111In-ABY-025, a second-generation affibody molecule with a fundamentally reengineered scaffold. J Nucl Med 2010;51:1131–8.
39. Tolmachev V, Wållberg H, Sandström M, Hansson M, Wennborg A, Orlova A. Optimal specific radioactivity of anti-HER2 Affibody molecules enables discrimination between xenografts with high and low HER2 expression levels. Eur J Nucl Med Mol Imaging 2011;38:531–9